5-17-2011

Flow-Enhanced Nonlinear Magnetophoresis for High-Resolution Bioseparation

Peng Li
University College Dublin

Aamer Mahmood
Birck Nanotechnology Center, Purdue University, amahmood@purdue.edu

Gil U. Lee
University College Dublin, gil.lee@ucd.ie

Langmuir

ARTICLE

pubs.acs.org/Langmuir

Flow-Enhanced Nonlinear Magnetophoresis for High-Resolution Bioseparation

Peng Li,[†] Aamer Mahmood,[‡] and Gil U. Lee[†,*]

[†]School of Chemistry and Chemical Biology, University College Dublin, Belfield, Dublin 4, Ireland

[‡]Birck Nanotechnology Center, Purdue University, West Lafayette, Indiana 47907, United States

Supporting Information

ABSTRACT: A new mode of transport is described that was capable of high-resolution separation of superparamagnetic materials from complex mixtures based on their size. Laminar flow and a rotating external magnetic field were applied to superparamagnetic beads assembled on a semiperiodic micromagnet array. Beads at the edge of the micromagnet array oscillated in-phase with the external magnetic field with an amplitude that decreased with increasing frequency, ω, until they reached an immobilization frequency, ω_i, where the beads stopped moving. Laminar flow along the edge of the array could be tuned to sweep the beads for which $\omega < \omega_i$ downstream at a velocity that increased with size while leaving beads for which $\omega > \omega_i$ undisturbed. Flow-enhanced nonlinear magnetophoresis (F-NLM) promises to enable multiple superparamagnetc bead types to be used in the fractionation of cells and implementation of diagnostic assays.

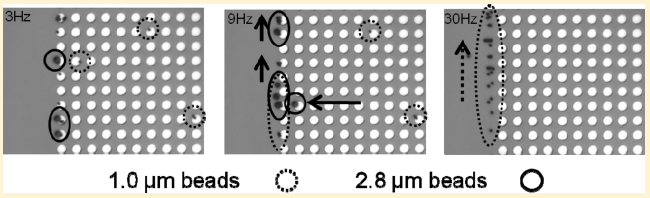

Our ability to understand and work with living systems on the molecular level is based on separation — bioseparation is the basis for determining the molecular state of a cell, or whole organism, and defines our capacity to utilize biologically derived molecules.[1] Currently, bioseparation is most often performed using liquid chromatography,[2] electrophoresis[3] or centrifugation,[4] which achieves separation by transporting an analyte relative to a stationary phase based on a physical or chemical property, such as surface chemistry, size, charge, or mass density. Although these techniques are able to separate analytes with a high resolution, it is widely recognized that they are slow and often difficult to implement.

One approach to increasing the speed of separation has been to use suspensions of micrometer-sized superparamagnetic beads to perform magnetically activated separation.[5,6] In this technique, the beads are functionalized with a receptor against a specific analyte and reacted with a sample using chemical schemes similar to those developed for affinity chromatography. The beads are removed from the sample in a high-gradient magnetic field and can then be resuspended after several washing steps due to their superparamagnetic properties. The increased speed of this technique results from rapid mass transport conditions produced by suspending the microbeads in the sample. Superparamagnetic beads have proven to be well suited for lab-on-a-chip separation of rare cell types[7,8] and highly sensitive bioanalytical measurements.[9−13] Current limitations of this technique are that separation is limited to a single step and magnetophoresis can lead to aggregation of the magnetic beads on the cells, which complicates the recovery of viable rare cell types.

We have recently demonstrated nonlinear magnetophoretic separation (NLM) of superparamagnetic beads on a micromagnet array using an external, rotating magnetic field to create a translating, periodic magnetic field.[14] Beads exposed to this translating potential energy landscape moved across the micromagnet array at a rate that was determined by the frequency of the external field rotation, ω, as well as the characteristic properties of the beads and array. At low frequencies, the magnetic beads became locked in the potential energy landscape and shuttled between adjacent magnets with a speed that was proportional to the velocity of the landscape. As the frequency was increased over a limit, the beads no longer remain in the local magnetic potential energy minima due to the force produced by hydrodynamic drag and became immobilized on the micromagnet. The frequency at which the beads start to become immobilized, the critical frequency (ω_c), was dependent on the size and magnetic moment of the superparamagnetic beads and micromagnets. NLM was used to isolate *B. globigii* and *S. cerevisiae* captured on 1.0 and 2.8 μm diameter magnetic beads functionalized with specific antibodies. This was achieved by sweeping ω from high to low frequencies to selectively separate bare microbeads and then microbeads that were bound to each of the microorganisms. Although NLM improves the resolution of linear magnetophoresis the relatively small number of beads that can be manipulated on a single chip limits its application.[14]

In this report, we examined the influence of hydrodynamic flow on NLM of superparamagnetic materials on a semiperiodic micromagnet array. NLM transport remained unchanged on the continuous micromagnet arrays at low hydrodynamic velocities

Received: December 29, 2010
Revised: March 16, 2011
Published: April 20, 2011

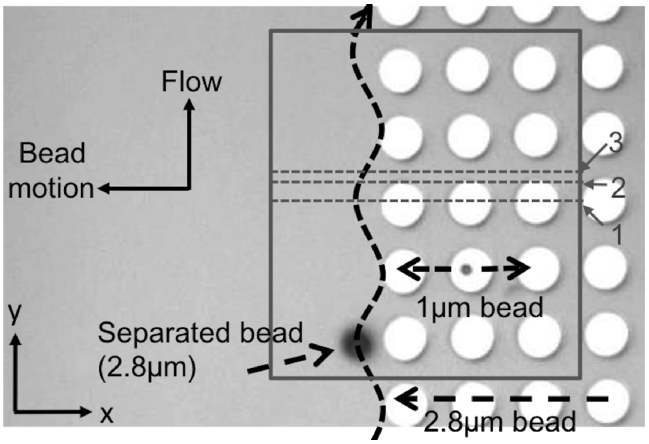

Figure 1. Top-view optical image of the micromagnet array (white circles) on which 1 and 2.8 μm diameter superparamagnetic beads (black circles) are suspended. The micromagnets have been magnetized in the x direction, the external magnetic field is rotated about the y axis, and a hydrodyamic flow is produced in the y direction. The motion of the beads under a 9 Hz rate of rotation of the external field has been drawn on the figure with dashed lines. The 2.8 μm beads move to the edge of the array and then allong its edge in a 100 μL/min flow. The 1 μm beads are locked on the array. The rectangle delineates the region in which the finite element calculation were preformed, which are described in the Discussion and Supporting Information. Line 1 — cross-section through the center line of the micromagnets. Line 2 — cross-section through the edge of the micromagnets. Line 3 — cross-section through the plane of symmetry between the micromagnets. Line 4 — cross-second along the edge of the micromagnets.

but the beads become displaced from the array as the flow rate increased. Unfortunately, the flow rate at which a bead was displaced from the continuous micromagnet array was not found to correlated with the size of the bead. The transport behavior of the beads was also studied on the edge of continuous micromagnet arrays, as shown in Figure 1. In the absence of flow the beads for which $\omega < \omega_c$ oscillated between a point on the edge of the micromagnets and a point in the area adjacent to the array with an amplitude that decreased with increasing frequency. Surprisingly, the motion of the beads along the edge of the array (y direction) was found to be a strong function of their size and external magnetic field frequency in flow, that is, a majority of beads were trapped on the edge of the micromagnet array at external field frequencies greater than a specific frequency, ω_i. The ω_i of a bead was found to increase with its size. As shown in Figure 1, a ω can be chosen at which the large beads with higher ω_i moved along the edge of the micromagnet array in the y direction, whereas the smaller beads with smaller ω_i remained trapped on the array. This study describes the transport of the beads on a semicontinuous micromagnet array as a function of bead size, flow rate, and external magnetic field rotation frequency.

EXPERIMENTAL SECTION

Microfabrication of the F-NLM Flow Chip with Micromagnet Array. The F-NLM chip was composed of an array of micromagnets embedded in a flow chamber with fluidic ports (Figure 1 of the Supporting Information). A positive photoresist based lift-off process was used to fabricate the cobalt micromagnets with a high degree of dimensional control. The micromagnet array was composed of 5.0 ± 0.1 μm diameter circular magnets arranged in a square lattice with an 8.0 ± 0.1 μm center-to-center distance. The micromagnets were created by thermally depositing 5 nm chromium, 70 nm cobalt, and 5 nm chromium on the patterned photoresist. After lift-off the resulting micromagnets were inspected with scanning electron microscopy and atomic force microscopy to determine their z and xy dimensions with a 1 and 10 nm resolution, respectively. The micromagnet arrays were subsequently coated with a 600 nm thick spin-on-glass (SOG) layer (Filmtronics, Butler, PA, USA) to provide chemical protection. The rectangular flow chamber around the magnets array was formed using a SU-8 (MicroChem, Newton, MA, USA) photolithographic process. The rectangular flow channel was 47 mm long, 7.8 mm wide, and 70 μm high. The microfluidics chamber was completed by using laser machining to form 1 mm diameter inlet and outlet holes in the micromagnet chip and then bonding a 170 μm thick quartz cover sheet to the SU-8 layer to from a closed chamber. The design of this flow chamber allowed the velocity of fluid flow to be set with 10% precision down the length of the chamber and the motion of the beads on the array to be characterized with an optical microscope.

F-NLM System. A rotating magnetic field orthogonal to the axis of flow on the F-NLM chip was generated with three electromagnets (Figure 1 of the Supporting Information).[14] The solenoids were composed of 570 coils surrounding a cylindrical iron core (ASTM A536 ductile iron) that had a diameter of 60 mm and length of 150 mm. Two synchronized sinusoidal signals with a 90° phase difference were generated with a two-channel function generator (Tektronix, Beaverton, Oregon, USA). This signal was amplified to the desired current using two programmable amplifiers (Kepco, Flushing, NY, USA) that was supplied to the electromagnets assembled in the x and z axes. This generated an elliptical, rotating magnetic field with amplitude of 48 and 29 G in the x direction and z directions, respectively. The uniformity of magnetic field generated by the electromagnets on the micromagnet array was >96% in the axial direction and >83% in the radial direction.

In a typical experiment, the sample was introduced into the flow chamber and then paused for one minute to allow the magnetic beads to be collected on the micromagnet array with the z direction electromagnet. Off-chip fluidic handling was used to control the flow on-chip and collect magnetic bead fractions. Syringe pumps (Chemyx, Stafford, TX, USA) were used to introduce sample and carrier fluids at a specified flow-rates between 20 and 300 μL/min. The Reynolds number (N_{re}) for a rectangular channel is $N_{re} = (\rho V_o D_h)/(\eta)$, where V_o is the average velocity of the liquid, D_h is the hydrodynamic diameter of the channel, and ρ and η are the density and viscosity of the fluid, respectively. N_{re} was of the order of magnitude of 10^{-7} for F-NLM, which is clearly deep in the creeping flow regime. F-NLM separation was executed after the beads were collected on the micromagnet array by introducing carrier fluid into the chamber at a defined flow rate and activating the rotating magnetic field at a specific frequency. Sample fractions separated at specific frequencies were collected using a valve manifold on the outlet port of the flow chamber.

The transport properties of the F-NLM device were characterized with an epi-illumination, optical microscope (Zeiss Axioskop 2, Welwyn Garden City, UK) with a 63× long-working distance lens. Images of the magnetic beads on the micromagnet array were acquired with a high-speed camera (Axiocam Hsm, Zeiss) capable of resolving the 1 μm diameter beads in a 140 × 110 μm field of view with 10 ms resolution. The velocity of the beads on the micromagnet array was measured by processing image sequences captured with the high-speed camera using the AxioVision time-lapse imaging software module. At least 10 beads were tracked for each experimental data point measurment presented in Figure 2. The critical rotation frequency of the beads was determined by defining the frequency at which the average bead velocity started to diverge from the velocity of the translating potential energy landscape,

Reagents. Two superparamagnetic beads were used in this study, i.e., carboxyl coated Dynabeads MyOne™ and M-270™ beads were

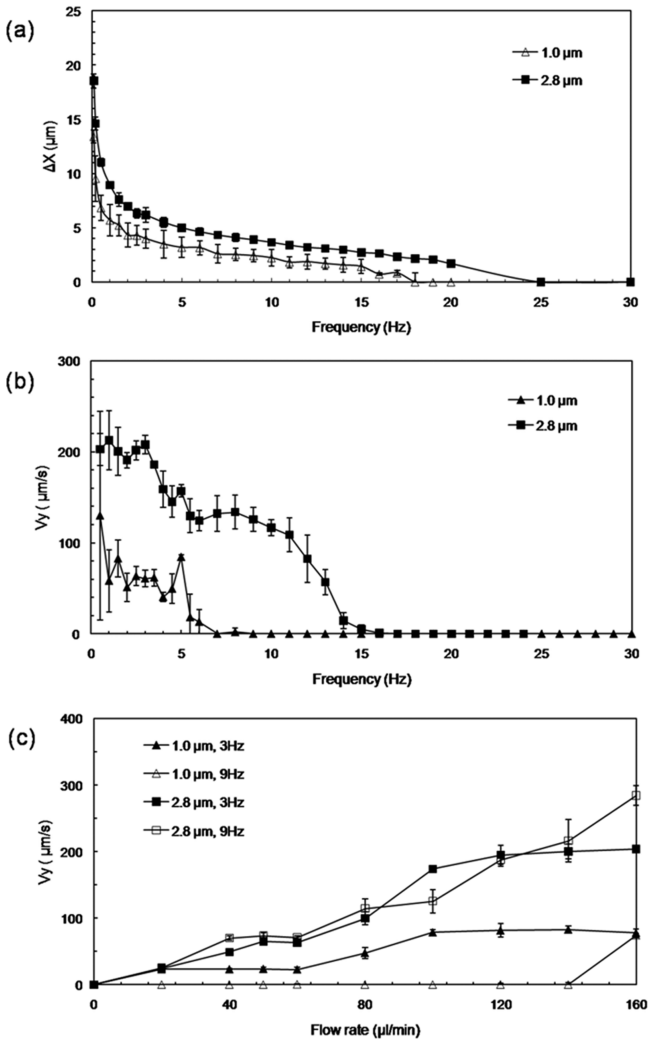

Figure 2. (a) Amplitude of oscilation of the beads, ΔX, on the edge of the micromagnetic array as a fucntion of rotation frequency, ω, of exteranl magnetic field without flow. (b) Speed of bead motion in the direciton of flow at the edge of the micromagent arrays, V_y, as a function of ω at $q = 100$ μL/min. The immobilization frequency of the beads was determined at the V_y equal to zero. (c) V_y of 1.0 and 2.8 μm beads on the edge of the magnetic array as a function of q and ω. The data points present the mean value and standard deviation (error bars) of 10 different beads.

purchased from Invitrogen (Carlsbad, CA, USA). The diameter of the beads were measured with scanning electron microscopy (S-4300 Hitachi, Krefeld, Germany) to be 1.0 and 2.8 μm respectively, with a coefficient of variation of the diameter of each bead less than 3%. The magnetic properties of beads were measured with SQUID magnetometry (Quantum Design, San Diego, CA, USA) at room temperature by dispersing the beads on a silicon substrate. The saturation magnetization of the beads was found to be 300 kA/m at 0.2 T, and the magnetic susceptibility (χ) of the 1.0 and 2.8 μm beads was 0.3 and 0.17, respectively. The beads were suspended in a 1 mM phosphate buffered saline solution with 0.5% Triton X-100 solution (PBST), which was also used as the carrier fluid.

RESULTS

Transport Behavior of the Superparamagnetic Beads on the Continuous Micromagnet Array. The motion of magnetic beads on the continuous micromagnet array was studied as a function bead radius (a), external magnetic field rotation frequency (ω), and flow rate (q) with an optical microscope. In the absence of flow, the beads were observed to move across the micromagnet arrays at low frequencies but became decoupled from the external magnetic field as the frequency increased, as previously reported.[14] The ω_c of the beads was defined as the frequency at which the average bead velocity, V_x, started to diverge from the velocity of the translating potential energy landscape. The velocity of the 1 and 2.8 μm diameter beads was measured as a function of the external magnetic field rotation frequency and ω_c was found to be 4.5 and 9 Hz, respectively. The frequency at which half of the magnetic beads were immobilized on the micromagnet array, which was define as the threshold frequency, ω_t, was found to be 5.5 and 12 Hz for the 1 and 2.8 μm diameter beads, respectively. The difference in the critical and threshold frequencies is attributed to the magnetization of the beads, which has been shown to vary by as much as 25% within a given lot.[15]

The behavior of the beads on the continuous micromagnet array was also studied as a function of flow rate. At a flow rate less than 140 μL/min very little change in NLM transport behavior could be detected, that is, the 1.0 and 2.8 μm beads began to become displaced from the micromagnet array at a flow rate of 160 and 140 μL/min, respectively. Unfortunately, each set of beads was displaced from the micromagnet array over a wide distribution of flow rates, which we also attribute the variation in their magnetization.

Transport Behavior of the Beads on the Edge of the Micromagnet Arrays. When the beads reached the edge of the micromagnetic array, they were observed to oscillate between the edge of the outer micromagnet and a position in the flow channel. Part a of Figure 2 presents the measured amplitude of this oscillation, ΔX, as a function of ω at $q = 0$, where ΔX was defined as the distance from the micromagnet to the center of the bead at the maximum distance from the micromagnet. Several trends assoicated with the bead motion can be identified in part a of Figure 2. First, ΔX decreased as ω increased. Second, the smaller beads had a smaller ΔX across all ω for which a diplacement could be measured. Third, there was a frequency at which ΔX became zero, which we defined as the point where the bead sticks to the surface of magnet and oscillates at its point of contact. The frequency at which ΔX became zero was 17 and 25 Hz for the 1 and 2.8 μm bead, respectively.

Part b of Figure 2 presents the velocity of the beads measured moving along the edge of the micromagnet array, V_y, as a function of ω at a flow rate of 100 μL/min. Several trends can be identified in these results. First, it appears that at ω less than the immobilization frequency, ω_i, the beads at the edge of an array moved with flow at a velocity that increased with their size. The magnitude of ω_i, which was defined as the frequency at which all of the beads were immobilized, was 7 and 16 Hz for the 1 and 2.8 μm beads, respectively. Second, at $\omega > \omega_i$ the beads slow down until they stop moving in the direction of flow.

Part c of Figure 2 presents the measurement of V_y as a function of flow rate at two frequencies of rotation of the external magnetic field for the two beads. These results confirm that the motion of the beads down the edge of the micromagnetic array was a nonlinear function of ω and that large beads moved faster than the small beads at a given flow rate. In fact, part c of Figure 2 illustrates that V_y was a linear function of flow rate when the frequency was less than ω_i. A flow rate of 100 μL/min was chosen for separation in this study as it produced a relatively large

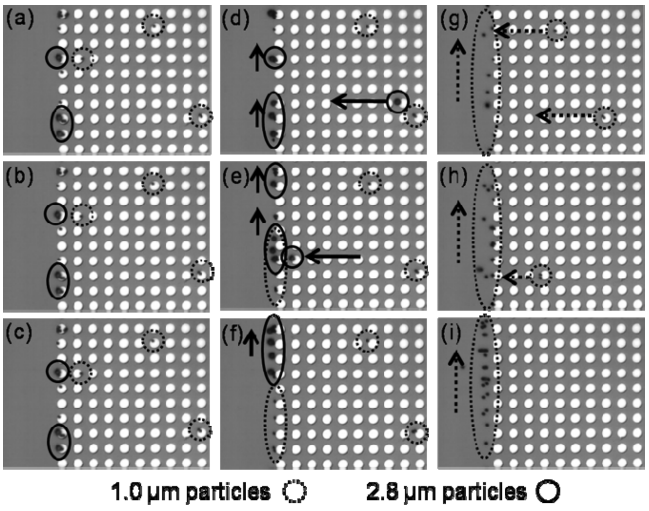

Figure 3. Sequence of screenshots of micrograph of showing the motion of a set magnetic beads on the edge of a micromagnet array at different separation frequencies. $q = 100\ \mu$m/min. Separation frequency is set to be 30 Hz in (a)−(c), 9 Hz in (d)−(f), 3 Hz in (g)−(i).

difference in V_y between the beads and avoided the range of flow rates where the beads on the array were swept away.

F-NLM Separation of the Magnetic Beads. Separation of the beads using F-NLM was demonstrated by stepping ω through a series of frequencies at a flow rate of 100 μL/min. Figure 3 illutrates a three step separation process. Initially, the external field freuency was set at 30 Hz, which exceeded the immobilization frequency of all the beads. Parts a, b, and c of Figure 3 show the beads at three time points and clearly illustrate taht the beads fixed on the edge of the micromagnet array. In a second stage the field frequency was decreased to 9 Hz where $\omega < \omega_{t,2.8\ \mu m} < \omega_{i,2.8\ \mu m}$ and $\omega > \omega_{i,1\ \mu m} > \omega_{t,1\ \mu m}$. Parts d, e, and f of Figure 3 demonstrate that the smaller 1 μm beads were fixed on the array, whereas the large beads moved across the array until they encounter an edge where they follow the direction of flow. In ths way, the larger beads were removed from the micromagnet array, whereas the 1 μm beads were trapped on the chip. In the last step, the frequency was decreased to 3 Hz where $\omega < \omega_{t,1\ \mu m}$ and $\omega_{i,1\ \mu m}$. Parts g, h, and i of Figure 3 illustrate that the small beads were diplaced from the chip and separated in the laminar flow. This demonstration of F-NLM illustrated that it was capable of separating magnetic beads of different size and magnetization using the frequency of rotation of the external magnetic field. Any remaining beads on the array could be displaced by increasing the laminar flow to sweep them downstream. A movie of the F-NLM separation of the 1 and 2.8 μm beads is presented in the Supporting Information.

DISCUSSION

Analysis of Motion of the Beads on a Continuous Micromagnet Array. The magnetic force applied to a superparamagentic bead by a rotating magnetic field on a continuous micromagnet array has been previously described as

$$F_x(x,t) = F_{mag} \sin(kx - \omega t) \quad (1)$$

where F_{mag} is the maximum magnetic force and $k = (2\pi)/(d)$ is a constant describing the spatial periodicity of the micromagnetic array.[14] The solution of the equation of motion for this bead reveals the bead's motion can be described as an over damped, nonlinear oscillator. The critical frequency for this oscillator is

$$\omega_c = \frac{\chi \mu_o \sigma_o H_{ext}}{18\eta}(2\pi\beta)^2 \exp(-2\pi\beta) \quad (2)$$

where μ_o is the permeability of free space, χ is susceptibility of magnetic bead, σ_o is an experimentally determined parameter representing the effective magnetic pole distribution on the array surface, H_{ext} is the magnitude of the external magnetic field, and β is the ratio of the bead radius, a, to the characteristic length scale of the array, d.

Over damped, nonlinear oscillators, exhibit two distinct transport regimes depending on the external drive frequency. When the external frequency was less than a critical frequency, the bead reached a stable position within a given trap in the energy landscape and moved at a constant horizontal velocity with a speed equal to the translation velocity of the landscape, $\omega(d)/(2\pi)$. Near the critical frequency, the bead lagged behind the local energy minima. Above the critical frequency, the beads began to slip with respect to the translating potential energy landscape. Physically the slipping was observed as an oscillatory rocking motion between adjacent magnets superimposed on a time-averaged linear velocity, which reduces to zero with increasing frequency at a rate defined by $[\omega - (\omega^2 - \omega_c^2)^{1/2}](d/2\pi)$.

The critical frequency of the 1 and 2.8 μm beads measured in this study was 4.5 and 9 Hz, respectively. The relative increase in critical frequencies with the size of bead was in agreement with eq 2 in terms of the experimentally determined parameters, that is, $\bar{\chi}$, a, and d. The critical frequencies were slightly higher than those measured in our previous study,[14] which can be attributed to differences in the physical properties of the micromagnets.

Analysis of the Motion of the Beads at the Edge of the Micromagnet Array. The magnetic field distribution at edge of a micromagnet array was simulated using finite element modeling. Figure 4 presents cross sections of the magnetic flux density, B, in an xz plane as a function of the orientation of the external magnetic field, θ. The magnitude of B has been presented in false color with a single scale used for all eight images. Clearly, the B profiles do not have a simple functional form thus the equation of motion of a bead cannot be solved analytically for F-NLM. However, several of the key elements of the F-NLM behavior can be understood in terms of the magnetic potential energy

$$U_m = -mB = -\frac{\chi v}{\mu_o}B^2 \quad (3)$$

and the force applied to the magnetic beads

$$F = (m\nabla)B = v\frac{3\chi}{\chi + 3}\nabla\frac{B}{2\mu_o} \quad (4)$$

where m is the magnetic moment of the bead and v is the volume of the bead.

The position of a magnetic bead on the edge of the array was drawn in Figure 4 at a point close to the highest local B, which represents the equilibrium position of the bead. Several observations can be drawn from Figure 4 that provide insight into the motion of the magnetic beads at the edge of the micromagnet array. First, the B distribution surrounding the micromagnets at the edge of the array had a form similar to that on the continuous

dx.doi.org/10.1021/la105126n |*Langmuir* 2011, 27, 6496–6503

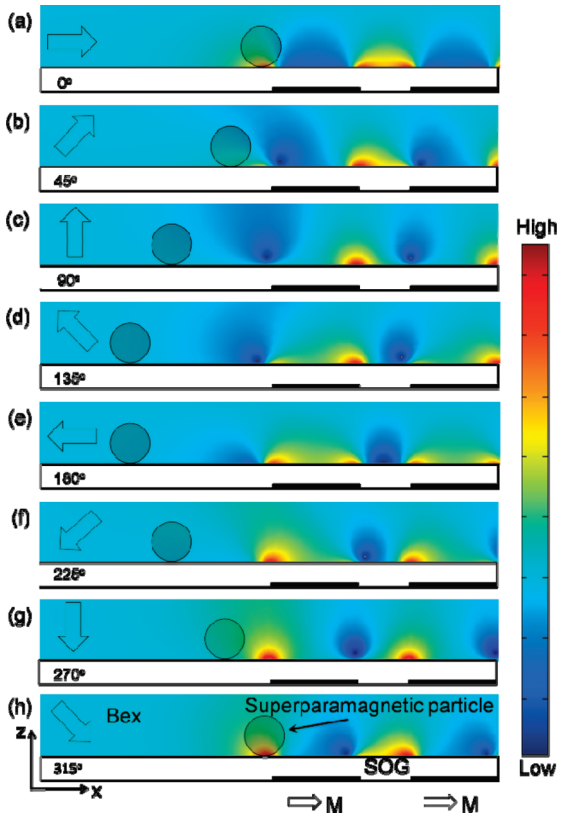

Figure 4. Finite element simulation of the normalized magnetic flux density in an *xz* plane through the center of the macro-magnets (shown as line 1 in Figure 1) presented as a function of θ. The magnitude of the external magnetic field, B_{ex}, was set to a value of 60 G. The position of micromagnets has been drawn as a black line at the bottom of each image relative to the 600 nm thick SOG layer. The micromagnets were set to have remnant flux density of 5000 G. For simplicity the surrounding materials were treated as nonmagnetic and the bead's inherent magnetization was not included in the simulation.

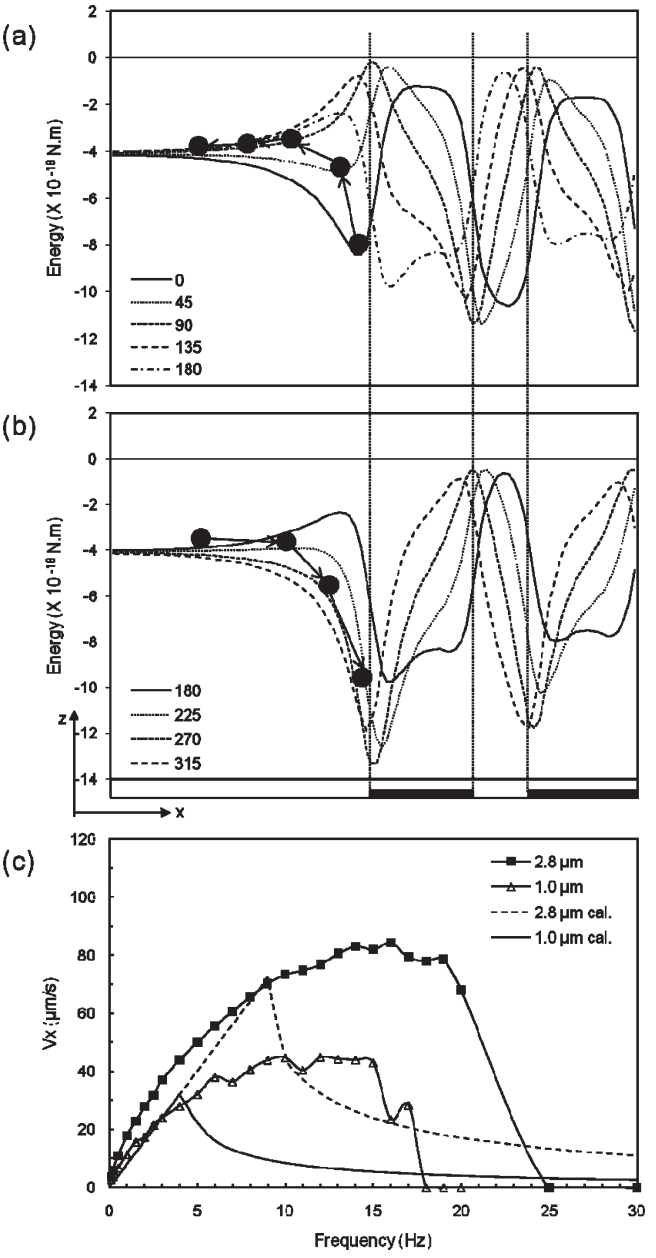

Figure 5. Magnetic potential energy at the edge of the micromagnet array presented as a function of θ along line 1 in Figure 1 and 0.5 μm above the SOG surface. Vertical lines have been used to identify the position of the micromagnets, which are also drawn on the graphs a black bars. (a) U_m for $0 < \theta < 180°$, (b) U_m for $180 < \theta < 315°$. Black bars in bottom: Position of micromagnets. The assumption has been made that U_m and $F_{m,y}$ can be calculated using the B at a single point x μm in front of the micrometer-magnets and 0.5 mm above the SOG surface. (c). Measured V_x F-NLM and calculated V_x NLM at the edge of the micromagnet array for the 2.8 and 1.0 μm beads as a function of ω. The NLM V_x was calculated as a function of ω from the solution of the overdamped harmonic oscillator.

array in many orientations of the external magnetic field. These B distributions allowed the beads to move from the continuous array onto the outer micromagnetic as θ was rotated counterclockwise from 0 to 360°. It also provided the driving force for the beads to enter the flow channel and oscillate between a point on the edge of the outer micromagnet and a point in the channel. Second, B did not have a maximum in the flow channel but was nearly constant at the electromagnet magnetic flux density of the external electromagnet, that is, 60 G. This B was significantly lower than the maximum B on the micromagnets but was higher than B on the left side of the outer micromagnet at θ values between 90° and 180°.

Parts a and b of Figure 5 resent calculations of the U_m for a 1.0 μm bead at particular values of θ along the center-line of the two micromagnets (line 1 of Figure 1). Part a of Figure 5 illustrates that the magnetic bead was trapped in a strong U_m minimum at the left edge of the outer micromagnet at $\theta = 0°$. The filled circles and arrows have been drawn on the energy profiles to illustrate the approximate position and direction of motion of a bead for $\omega < \omega_t$. At $\theta = 90°$ the bead moved into the channel in a local U_m minimum. At the higher θ, the bead continued to move away from the micromagnet array in an almost flat U_m profile until $\theta = 180°$, where the bead reversed direction and moved toward the local energy minimum that appeared at the left side of the outer micromagnet, as shown in part b of Figure 5. The fact that the magnetic bead moved in an relatively flat U_m rather than a deep U_m minimum for $90° < \theta < 180°$ is the key to its unique behavior at the edge of the micromagnet array in F-NLM.

Part c of Figure 5 presents the measured V_x for F-NLM as well as the calculated V_x for NLM of the 1.0 and 2.8 μm beads as a

dx.doi.org/10.1021/la105126n |*Langmuir* 2011, 27, 6496–6503

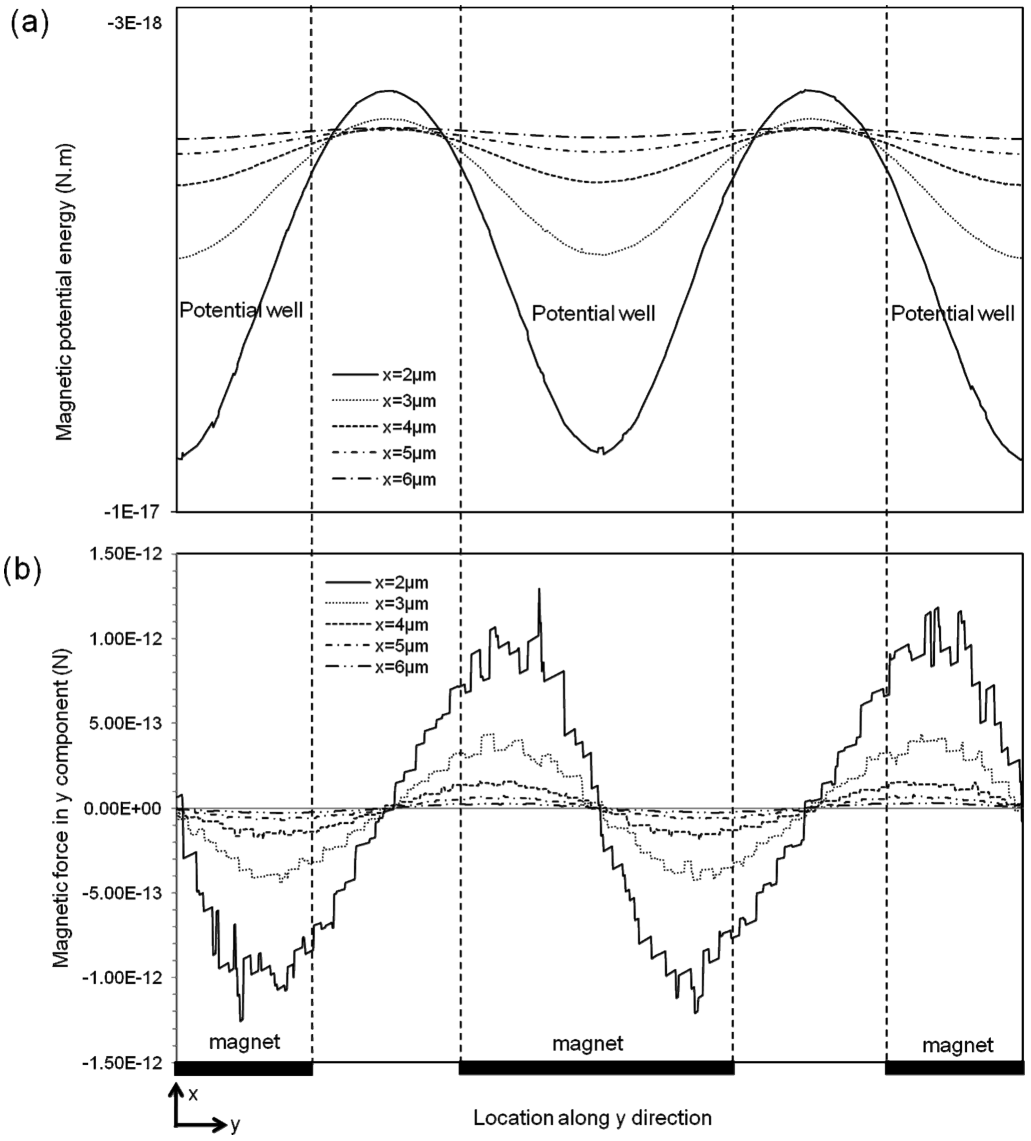

Figure 6. Magnetic potential energy (a) and force in the *y* direction (b) experienced by a 1 μm particle in a line *x* μm in front of the micrometer-magnets at the edge of the array for $\theta = 0°$. The assumption has been made that U_m and $F_{m,y}$ can be calculated using the *B* at a single point *x* μm in front of the micrometer magnets and 0.5 μm above the SOG surface. The *B* fields were determined using 3D finite element analysis (results presented Supporting Information).

function of ω. The velocity-frequency behavior of the beads in F-NLM had similarities to NLM, that is, the velocity of the beads increased at a rate proportional to $\omega(d)/(2\pi)$ until the external magnetic field frequency reached ω_c. However, at frequencies above ω_c the F-NLM velocity of the beads remained approximately constant until ω_t was reached. The constant V_x of the F-NLM beads for $\omega_c < \omega < \omega_t$ appears to result from the fact that the U_m was weak in the channel next to the micromagnet array for $90° < \theta < 180°$.

The *B* distribution was also calculated in three-dimensions for a 5 × 3 micromagnet array at the edge of the array, that is, area enclosed by the rectangle in Figure 1, and the results are presented in the in the Supporting Information. The *B* distributions in *xz* planes along the edge of the micromagnets (line 2 in Figure 1) and the plane of symmetry between the micromagnets (line 3 in Figure 1) have a similar form to that observed along the center of the micromagnets (line 1 in Figure 1). Thus, the beads experience dynamic magnetic flux densities similar to those presented in Figure 4 as they move down the edge of the array although the magnitude and relative position of maximum of *B* change significantly. This was consistent with the motion of the beads illustrated in Figure 1 in which the beads moved along the edge of the micromagnet array in a trajectory that varied in *x*.

F-NLM Separation of the Magnetic Beads. A movie of the F-NLM separation of the 1 and 2.8 μm beads is presented in the Supporting Information. This movie demonstrated that at $\omega_{i,1.0\ um} < \omega < \omega_{t,2.8um} < \omega_{i,2.8um}$ the 2.8 μm beads rapidly moved off and down the edge of the micromagnet array. If the frequency was then shifted to $\omega < \omega_{t,1.0\ um} < \omega_{i,1.0um}$ the remaining 1 μm beads rapidly moved off micromagnet array and down its edge resulting in complete separation of these two bead populations in the microscopic field of view. It was striking that this separation process worked even at high densities of the microbeads in which the beads can be seen to collide with each other and form aggregates.

dx.doi.org/10.1021/la105126n |*Langmuir* 2011, 27, 6496–6503

This movie highlighted the significant difference in V_y of the two bead populations as they move along the edge of the micromagnetic array. The V_y of the beads was observed to increase with radius at frequencies less than ω_t, that is, the velocity of the 1 and 2.8 μm bead in part c of Figure 2 was approximately 60 and 180 μm/s, respectively, for a flow rate of 100 μL/min at ω = 3 Hz. The relationship between bead diameter and its velocity resulted in large part from the hydrodynamic drag that the bead experienced at the surface of the chamber. That is, the hydrodynamic drag force experienced by a sphere in laminar flow at a surface can be calculated using Stokes equation

$$F_h = -6\pi\mu V f_d a \quad (5)$$

where V is the fluid velocity at the center of the bead and the drag coefficient $f_d = (1+(9)/(16)((a)/(h)))$ is a function of bead radius (a) and the height of the bead above the surface of the chamber, h.[16] Because the beads were small relative to the dimensions of the flow chamber the flow profile surrounding the beads was almost linear with velocity, that is, the calculated hydrodynamic velocity was 57 and 160 μm/s at a at the center of the 1.0 and 2.7 μm beads, respectively. Thus, it appears the beads moved along the edge of the micromagnet array at a velocity that increased with their radius because laminar flow produced a linear relationship between the size of the bead and the fluid velocity at the center of the bead.

Figure 6 presents the results of calculations of the magnetic potential energy, U_m, and y component of the magnetic force, $F_{m,y}$, of a 1 μm bead at a specific x and y position in front of the edge of the micromagnetic for $\theta = 0°$. Part a of Figure 6 confirmed that the potential energy was lowest at the center of the micromagnet (line 1 in Figure 1) and that the magnitude of the energy minimum decreased rapidly as the bead moved away from the micromagnet in the x direction. Part b of Figure 6 demonstrated that $F_{m,y}$ acted to center the bead on the micromagnet and rapidly decreased in magnitude as x increased. Reflection on the motion of a bead at the edge of the micromagnet array suggests that ω_i was determined by the ΔX of the bead at which the restraining force produced by the magnetic field, $F_{m,y}$, exceeds the hydrodynamic force $F_{h,y}$. The hydrodynamic force applied to the 1.0 and 2.8 μm beads for q = 100 μm/s can be calculated using eq 5 to be 1.7 and 13 pN respectively if we assume h = 0. Part b of Figure 6 suggests the hydrodynamic force is equivalent to at magnetic force at $\Delta X \approx 2$ μm, which is in qualitative agreement with the observed behavior of the beads.

CONCLUSIONS

We have described for the first time the separation of superparamagnetic beads on a semicontinuous micromagnet array in hydrodynamic and rotating magnetic fields, as shown in Figure 1. The transport of the beads at the edge of the continuous micromagnetic array was characterized by: 1) the nonlinear oscillation of the beads in the x direction on the edge of the micromagnets determined by the external magnetic field rotation frequency, ω, the size of the bead, and the magnetization of the bead; and 2) linear motional along the edge of the micromagnetic array in the y direction at a velocity that increase with the size the bead. Insight into this behavior was gained from finite element analysis of the magnetic flux density, B, produced by the micromagnets at the edge of the array as a function of external magnetic field orientation, θ. As θ increased from 0 to 180° the beads traveled from a strong energy minimum, U_m, on the edge of the outer micromagnet into the flow channel where a weak local U_m minimum formed. As θ increased from 180 to 360° the beads moved back to the edge of the micromagnet where a strong U_m minimum redeveloped. The motion of the beads between these two states led to nonlinear x direction transport behavior, that is, the magnitude of displacement of the beads decreasing with increasing external magnetic field rotation frequency, ω, until an immobilization frequency, ω_i, was reached. This nonlinear behavior allowed the beads to be separated with high-resolution, as ω_i was a strong function of bead size and flow rate. The beads moved along the edge of the micromagnet array in the flow field when $\omega < \omega_i$ at a velocity that was proportional to their size. This transport behavior also resulted from the weak local U_m minimum that is created at the edge of the micromagnet array, which acted as a magnetic trap strongly influenced by the hydrodynamic flow field. In conclusion, we have demonstrated that F-NLM can be used to separate superparamagnetic based on size. F-NLM promises to enable rapid, high-resolution separation of multiple analytes bound to superparamagnetic beads of defined size that have been labeled with specific antibodies. This technique may prove useful for multiplexing diagnostic assays and simultaneously separating multiple cell populations based on superparamagentic beads of defined size.

ASSOCIATED CONTENT

Supporting Information. Information regarding flow-enhanced nonlinear magnetophoresis system, the 3D magnetic field distribution on the micriomagnetic array, and the separation of the 1 and 2.8 μm beads. This material is available free of charge via the Internet at http://pubs.acs.org.

AUTHOR INFORMATION

Corresponding Author
*E-mail: gil.lee@ucd.ie.

ACKNOWLEDGMENT

The authors acknowledge the Science Foundation of Ireland (Grants 08/RP1/B1376 and NAP158) and IRCSET for providing financial supporting for this work. We also thank Joe O'Brien and Mark Platt for helpful discussions.

REFERENCES

(1) Belter, P. A.; Cussler, E. L.; Hu, W.-S., *Bioseparations: Downstream Processing for Biotechnology*; Wiley: New York, 1988; p xvi, 368 p.

(2) Svedberg, T.; Fahraeus, R. A new method for the determination of the molecular weight of the proteins. *J. Am. Chem. Soc.* **1926**, *48* (1), 430–438.

(3) Tiselius, A. A new apparatus for electrophoretic analysis of colloidal mixtures. *Trans. Faraday Soc.* **1937**, *33* (1), 0524–0530.

(4) Tiselius, A.; Pedersen, K. O.; Svedberg, T. Analytical measurements of ultracentrifugal sedimentation. *Nature* **1937**, *140*, 848–849.

(5) Kemshead, J. T.; Gibson, F. J.; Ugelstad, J.; Rembaum, A. A flow system for the invitro separation of tumor-cells from bone-marrow using monoclonal-antibodies and magnetic microspheres. *Proc. Am. Assoc. Cancer Res.* **1983**, 24, (Mar), 217-217.

(6) Kemshead, J. T.; Ugelstad, J.; Rembaum, A.; Gibson, F. Monoclonal-antibodies attached to microspheres containing magnetic compounds, used to remove neuro-blastoma cells from bone-marrow taken for autologous transplantation. *Eur. J. Cancer Clin. On.* **1982**, *18* (10), 1043–1043.

(7) Tibbe, A. G. J.; Grooth, B. G. d.; Greve, J.; Liberti, P. A.; Dolan, G. J.; Terstappen, L. W. M. M. Optical tracking and detection of immunomagnetically selected and aligned cells. *Nat. Biotechnol.* **1999**, *17* (12), 1210–1213.

(8) Han, K. H.; Frazier, A. B. Paramagnetic capture mode magnetophoretic microseparator for high efficiency blood cell separations. *Lab Chip* **2006**, *6* (2), 265–73.

(9) Oh, B. K.; Park, S.; Millstone, J. E.; Lee, S. W.; Lee, K. B.; Mirkin, C. A. Separation of tricomponent protein mixtures with triblock nanorods. *J. Am. Chem. Soc.* **2006**, *128* (36), 11825–11829.

(10) Osterfeld, S. J.; Yu, H.; Gaster, R. S.; Caramuta, S.; Xu, L.; Han, S. J.; Hall, D. A.; Wilson, R. J.; Sun, S. H.; White, R. L.; Davis, R. W.; Pourmand, N.; Wang, S. X. Multiplex protein assay based on real-time magnetic nanotag sensing. *Proc. Natl. Acad. Sci. U.S.A.* **2008**, *105* (52), 20637–20640.

(11) Bruls, D. M.; Evers, T. H.; Kahlman, J. A. H.; van Lankvelt, P. J. W.; Ovsyanko, M.; Pelssers, E. G. M.; Schielpen, J. J. H. B.; de Theije, F. K.; Verschurne, C. A.; van der Wijk, T.; van Zon, J. B. A.; Dittmer, W. U.; Immink, A. H. J.; Nieuwehnuis, J. H.; Prins, M. W. J. Rapid integrated biosensor for multiplexed immunoassays based on actuated magnetic nanoparticles. *Lab Chip* **2009**, *9* (24), 3504–3510.

(12) Godino, N.; Snakenborg, D.; Kutter, J. P.; Emmeus, J.; Hansen, M. F.; Munoz, F. X.; de. Campo, F. J. Construction and characterization of a modular microfluidic system: coupling magnetic capture and electrochemical detection. *Microfluid. Nanofluid.* **2010**, *8* (3), 393–402.

(13) Gijs, M. A. M.; Lacharme, F.; Lehmann, U. Microfluidic applications of magnetic particles fo biological analysis and catalysis. *Chem. Rev.* **2010**, *110* (3), 1518–1563.

(14) Yellen, B. B.; Erb, R. M.; Son, H. S.; Hewlin, R.; Shang, H.; Lee, G. U. Traveling wave magnetophoresis for high resolution chip based separations. *Lab Chip* **2007**, *7* (12), 1681–1688.

(15) van Ommering, K.; Lamers, C. C. H.; Nieuwenhuis, J. H.; van Ijzendoorn, L. J.; Prins, M. W. J. Analysis of individual magnetic particle motion near a chip surface. *J. Appl. Phys.* **2009**, *105* (10), 10.

(16) Happel, J.; Brenner, H. *Low Reynolds Number Hydrodynamics*; Prentice-Hall: Englewood Cliffs; 1065.